MEDICAL IMAGING

An improved method for automated calculation of the water-equivalent diameter for estimating size-specific dose in CT

Choirul Anam[1] | Fahmi Rosydiansyah Mahdani[1] | Winda Kusuma Dewi[1] |
Heri Sutanto[1] | Pandji Triadyaksa[1] | Freddy Haryanto[2] | Geoff Dougherty[3]

[1]Department of Physics, Faculty of Sciences and Mathematics, Diponegoro University, Central Java, Indonesia

[2]Department of Physics, Faculty of Mathematics and Natural Sciences, Bandung Institute of Technology, Bandung, West Java, Indonesia

[3]Department of Applied Physics and Medical Imaging, California State University Channel Islands, Camarillo, CA, USA

Correspondence
Choirul Anam, Department of Physics, Faculty of Sciences and Mathematics, Diponegoro University, Jl. Prof Soedarto, SH Tembalang, Semarang 50275, Central Java, Indonesia.
Email: anam@fisika.fsm.undip.ac.id

Funding information
Diponegoro University, Grant/Award Number: 118-08/UN7.6.1/PP/2021

Abstract

Purpose: The aim of this study is to propose an algorithm for the automated calculation of water-equivalent diameter (D_w) and size-specific dose estimation (SSDE) from clinical computed tomography (CT) images containing one or more substantial body part.

Methods: All CT datasets were retrospectively acquired by the Toshiba Aquilion 128 CT scanner. The proposed algorithm consisted of a contouring stage for the D_w calculation, carried out by taking the six largest objects in the cross-sectional image of the patient's body, followed by the removal of the CT table depending on the center position (*y*-axis) of each object. Validation of the proposed algorithm used images of patients who had undergone chest examination with both arms raised up, one arm placed down and both arms placed down, images of the pelvic region consisting of one substantial object, and images of the lower extremities consisting of two separated areas.

Results: The proposed algorithm gave the same results for D_w and SSDE as the previous algorithm when images consisted of one substantial body part. However, when images consisted of more than one substantial body part, the new algorithm was able to detect all parts of the patient within the image. The D_w values from the proposed algorithm were 9.5%, 15.4%, and 39.6% greater than the previous algorithm for the chest region with one arm placed down, both arms placed down, and images with two legs, respectively. The SSDE values from the proposed algorithm were 8.2%, 11.2%, and 20.6% lower than the previous algorithm for the same images, respectively.

Conclusions: We have presented an improved algorithm for automated calculation of D_w and SSDE. The proposed algorithm is more general and gives accurate results for both D_w and SSDE whether the CT images contain one or more than one substantial body part.

1 | INTRODUCTION

With the continually increasing use of CT worldwide,[1,2] and with the concern regarding the probability of cancer occurrence in the future induced by relatively high radiation doses from CT, especially in pediatric patients,[3,4] an accurate estimation of CT dose is important. Nowadays, the most widely used metrics of CT dose are computed tomography dose index (CTDI) and dose length product (DLP).[5] However, it has been shown that CTDI and DLP do not assess patient dose, but rather assess scanner output metrics independent of patient geometric-size and tissue attenuation.[6] They are both influenced by the input scanner settings such as tube current, tube voltage, rotation time, beamwidth, and pitch.[5]

The CTDI metric was initially proposed to improve the multiple scan average dose (MSAD) metrics for quantifying the CT scanner output dose.[7] Subsequent modifications of CTDI such as $CTDI_{100}$, $CTDI_w$, and $CTDI_{vol}$ were developed to facilitate the demand for CT dosimetry management.[8,9] Basically, CTDI measurement can be accomplished by integrating a single scan dose profile along the longitudinal axis (z-axis), and then dividing it by the beam collimation. $CTDI_{100}$, which is measured by a 100-mm-long pencil ionization chamber, raises questions about its efficiency in wide beam CT.[10] This is because a length of 100 mm is deemed insufficient to accumulate the scattered dose distribution. The way to overcome this problem is to extend the phantom length to a minimum of 45 cm and to use a small volume ion chamber to reach dose equilibrium.[11,12]

The $CTDI_{100}$ varies across the field of view (FOV). In case of body CT imaging, for instance, the $CTDI_{100}$ is typically a factor or two higher at the surface ($CTDI_{100,p}$) than at the center ($CTDI_{100,c}$). The average $CTDI_{100}$ across the FOV is characterized by the weighted CTDI
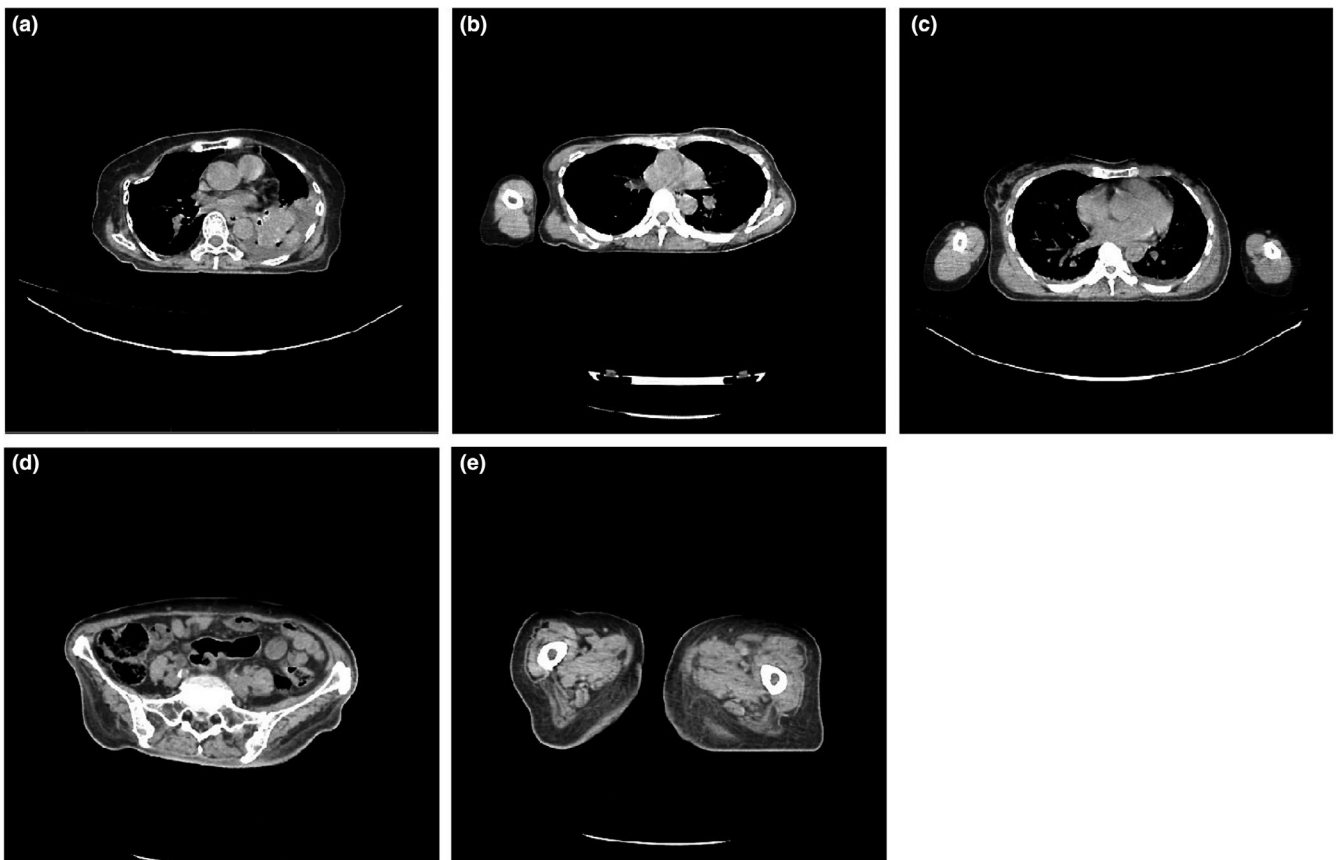

FIGURE 1 Examples of various axial images used in this study. (a) chest region with both arms raised up, (b) chest region with one arm placed downwards, (c) chest region with both arms placed downwards, (d) pelvic region consisting of one substantial object, and (e) lower extremities (legs) consisting two separated areas. Images (a) and (d) show one substantial object, while images (b), (c), and (e) show more than one substantial separated objects

(CTDI$_w$).[13] To represent output dose involving a series of scans, it is important to take into account any overlaps or gaps between the x-ray beams from consecutive rotations of the x-ray source. This is characterized with volume CTDI (CTDI$_{vol}$).[13,14] The CTDI$_{vol}$ is measured using a standardized polymethyl methacrylate (PMMA) phantom, either with a fixed diameter of 16 cm to express the patient's head or a diameter of 32 cm and length of 15 cm to express the patient's body.[13,14] However, both phantoms do not reflect the diversity of patient size. In a clinical setting, the geometrical size of patients can run from less than 10 cm for a newborn child to more than 35 cm for an obese adult patient.[15,16] In addition, the PMMA phantom was specially designed to be homogenous, and does not reflect the heterogeneous nature of the human body. For these reasons, CTDI$_{vol}$ reflects a proper and consistent index of scanner output only.

A new dose metric, the size-specific dose estimate (SSDE), was introduced[17] to fully accommodate the patient size and the scanner setting. Patient size was described by the effective diameter (D$_{eff}$), which can be obtained from both the anterior posterior (AP) and lateral (LAT) dimensions. SSDE is calculated by normalizing CTDI$_{vol}$ with a size conversion factor (f_{size}) taken from AAPM 204.[17] However, D$_{eff}$ does not account for the attenuation effects of the body's constituent materials[18] nor their respective densities,[19] and therefore it is not accurate for dose estimation.

An improved, more accurate metric to include both patient size and tissue attenuation, the water-equivalent diameter (D$_w$) was proposed.[20,21] D$_w$ can be calculated either from CT localizer radiographs or from axial CT images. The attenuation values from axial CT images can be calculated directly by averaging the CT number in a region of interest (ROI) containing that object, while calculation from CT localizer radiographs can be performed by properly calibrating the pixel values in terms of water attenuation.[22] Daudelin et al.[23] have evaluated the methods to quantify patient attenuation from CT localizer radiographs. Localizer-based D$_w$ calculation is highly affected by minification or magnification of the LAT dimension due to mis-positioning of the patient from the iso-center.[20] Thus, measurement of D$_w$ using reconstructed axial CT images provides a more accurate result.[20]

An accurate automated approach to finding D$_w$, in order to obtain accurate patient dose, is in great demand.[24–30] Anam et al.[25] proposed a fully automated method to calculate D$_w$ in a phantom and in human anatomic regions using a region of interest (ROI) automatically fitted to the patient border. The automated calculation produced an excellent correlation to the manual calculation (R^2 = 0.999). Özsoykal et al.[26] designed a patient contour upon the exclusion of irrelevant objects such as the CT table or clothes from the original image. The threshold value was then determined via trial and error until a complete segmentation of the body contour
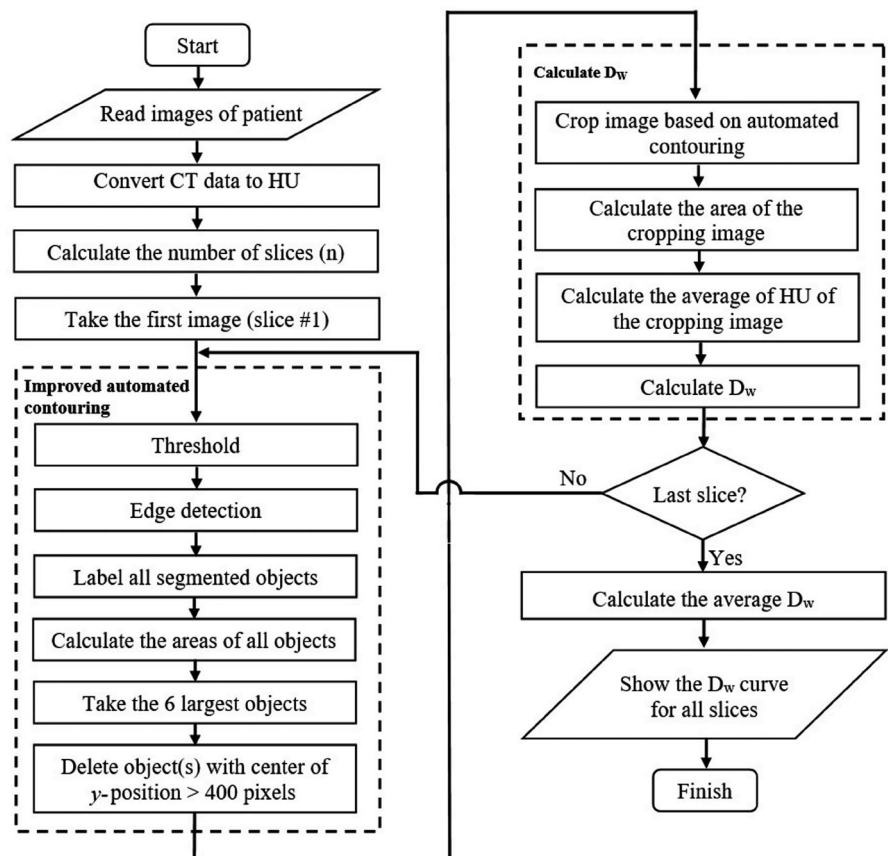

FIGURE 2 Flowchart of the proposed algorithm

was achieved. Gharbi et al.[27] also successfully proposed an automated method to measure D_w and SSDE based on the Fuzzy C-means classification algorithm and edge detection. Recently, Juszczyk et al.[24] proposed an automated segmentation of patient images to calculate D_w and SSDE using a convolutional neural network (CNN) and reported accurate results. The algorithms were effectively designed to calculate D_w based on segmentation of the largest object.[28] Previous algorithms failed to segment the patient body in the case of images which consisted of more than one substantial separated body part, for example, chest images when the patient's arm was within the image and separated from the chest, and the lower extremities images where the two legs are separated. This inaccuracy of patient image segmentation led to an underestimate of D_w and an overestimate of SSDE. Therefore, we propose an improvement of the automated D_w calculation which will accurately measure SSDE even in thoracic examinations which include the patient's arms and lower extremities examinations which include separated legs. Our algorithm is expected to result in a general and more accurate patient segmentation from images whether they consist of one or more substantial separated objects. Thus, the estimate of patient

doses (SSDE) will be more accurate and robust, so that the dose optimization through the diagnostic reference level (DRL) on the basis of SSDE can be increased.

2 | METHODS

2.1 | Images

This was a retrospective study on datasets from a hospital where anonymization and confidentiality were performed. All datasets were obtained from a multi-detector computed tomography (MDCT), the Toshiba Aquilion 128, between August 2014 and December 2014. The dataset consisted of axial images of adult patients who had undergone chest, pelvic, and lower extremities CT examinations. The chest datasets were classified into three groups: 40 datasets with both arms raised (Figure 1a), 40 datasets with one arm placed downwards (Figure 1b), and 20 datasets with both arms placed downwards (Figure 1c). The pelvic (one substantial object [Figure 1d]) and lower extremities (with two separated legs [Figure 1e]) each consisted of 38 datasets.
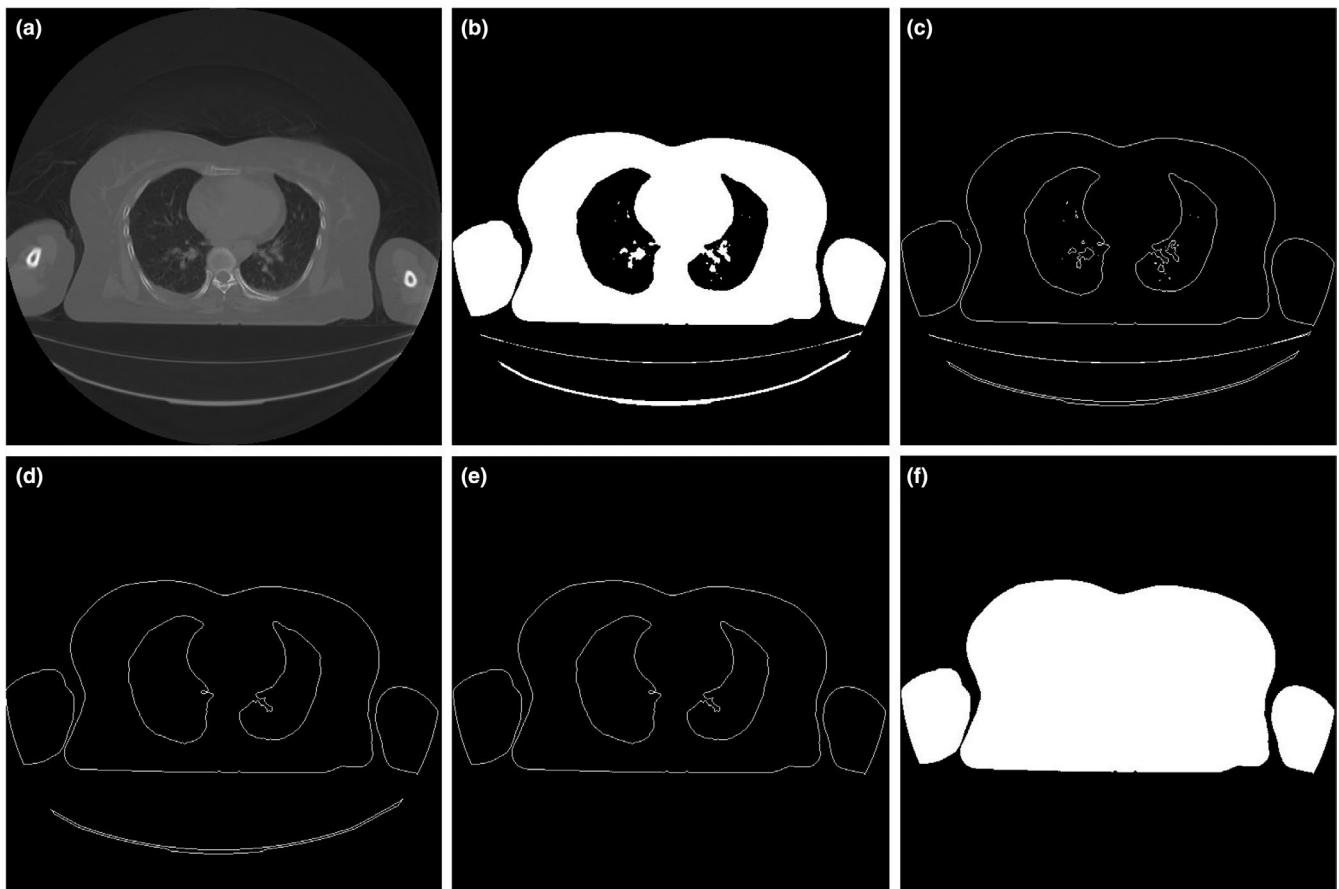

FIGURE 3   Proposed automated contouring stages: (a) initial image after converting CT data into HU, (b) binary image as a result of thresholding, (c) result of edge detection, (d) image showing the 6 largest objects including the patient table, (e) patient boundary after table removal, and (f) result of automated contouring after assigning all pixels within patient boundary with a value of 1

2.2 | Proposed algorithm

The flowchart of the proposed algorithm is presented in Figure 2. The current method is a modification of our previous algorithm.[25] The previous automated D_w calculation employed a threshold operation using a HU of −200, edge detection, and setting the largest object as the patient boundary.[25] It agreed well (to within <0.5%) with the manual calculation.

For images involving multiple parts of the patient's body, the contouring process based on the largest object produces an inaccurate estimate of D_w. Therefore,
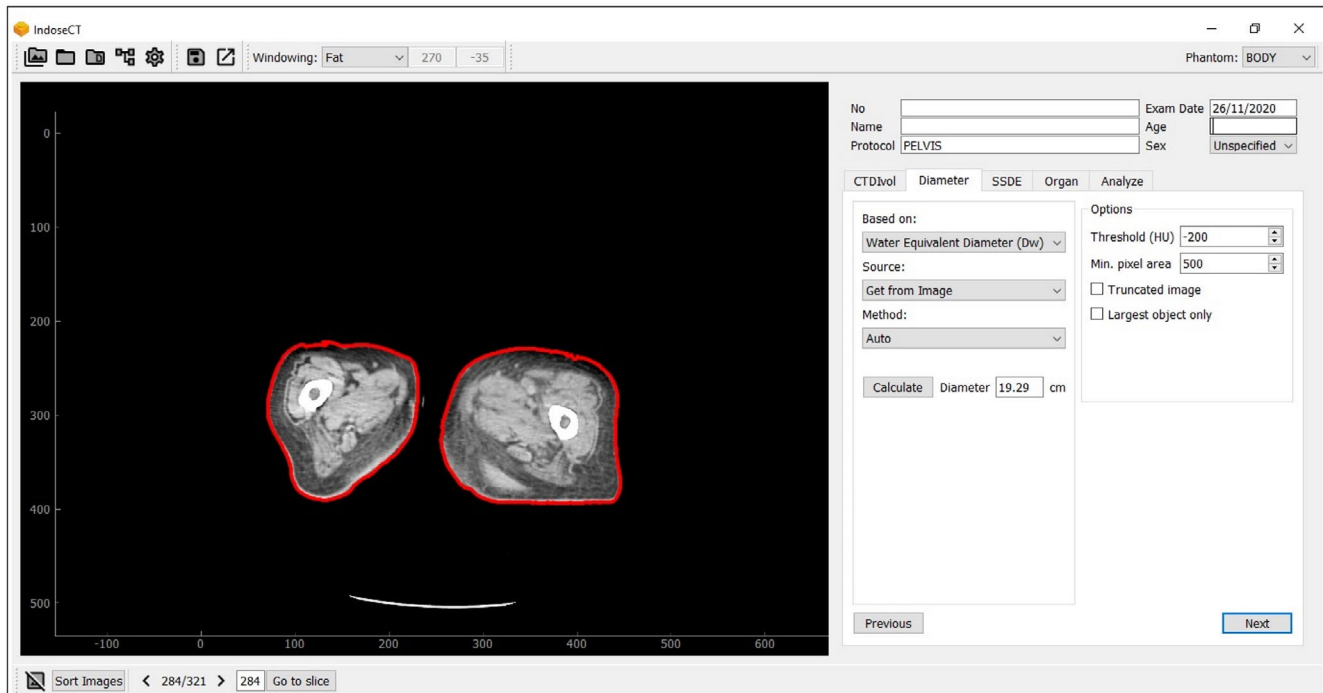
(a)
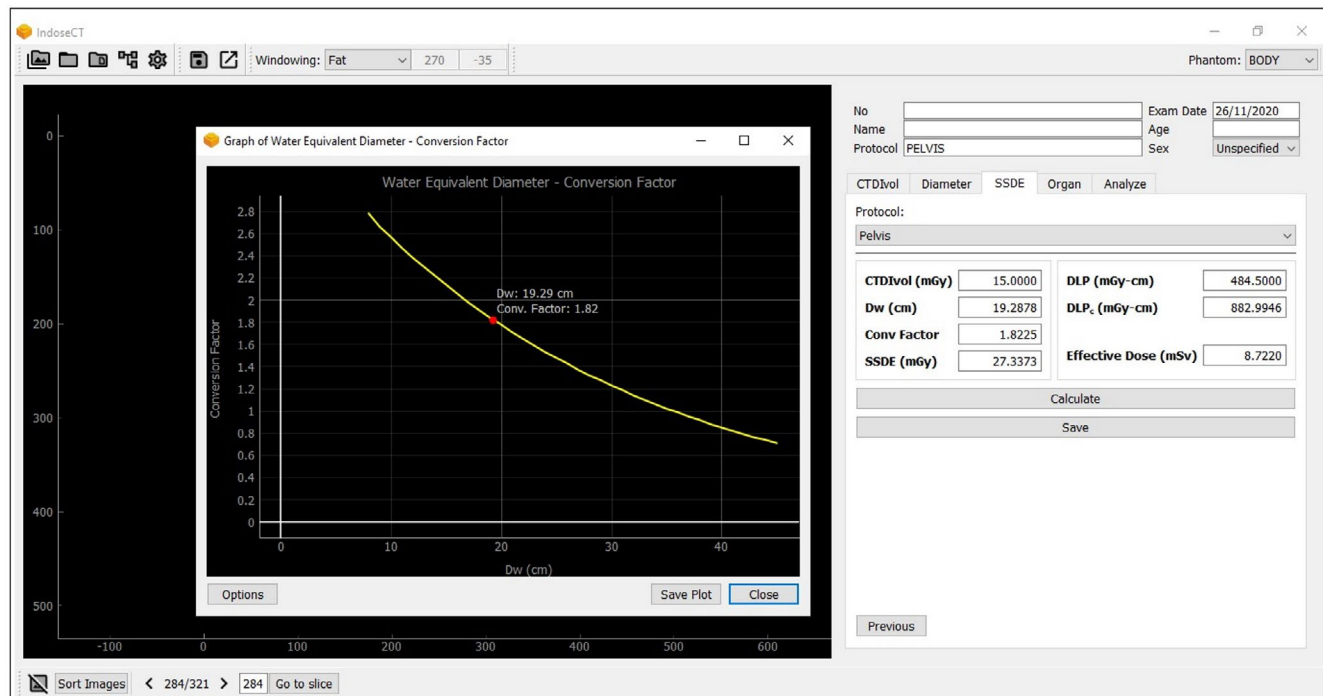
(b)

FIGURE 4 The screen displays of the graphical user interface (GUI) of IndoseCT showing (a) D_w calculation and (b) SSDE calculation
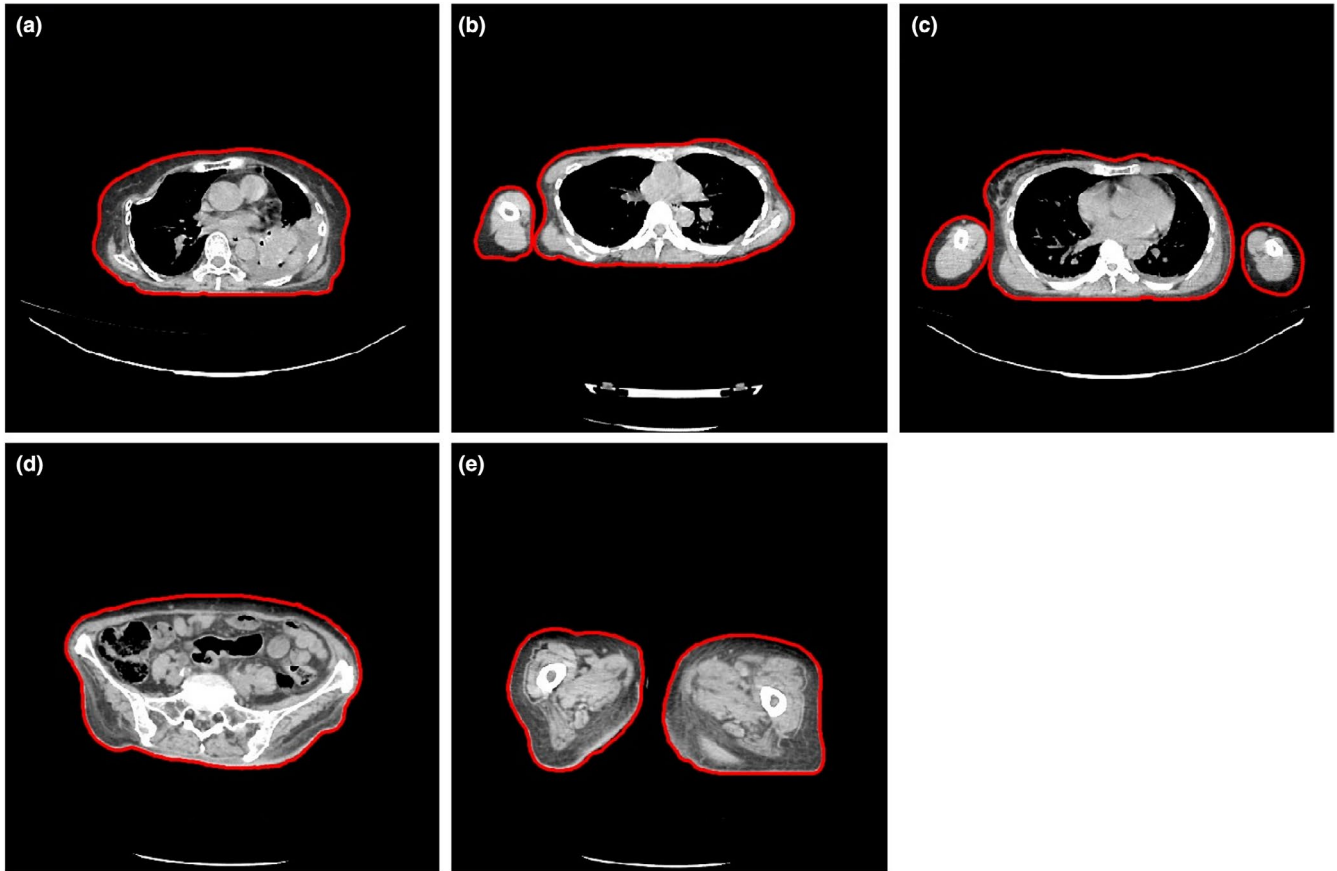
FIGURE 5 Images showing results of contouring based on the new improved algorithm. It shows that all of the patient's body in the image can be fully contoured whether the images containing one or more than one substantial separated objects

instead of using the largest body part as the patient border, the current method uses the six largest body parts. If the image consists of more than one substantial body part, the algorithm successfully detects the edges of all these body parts. On the other hand, if the image consists of only one substantial body part, then the five smaller detected body parts located within the one largest body part will be united into one large body part.

The stages of the automatic contouring are shown in Figure 3. A threshold operation was applied to the patient image (Figure 3b) after converting the DICOM image into HU. The perimeter of the patient was identified using edge detection (Figure 3c) and each object was labeled. The areas of all the objects were calculated, and the six largest objects were identified (Figure 3d). The patient table, however, is often detected at this stage.[18,31] To remove it, we determined the center positions (*y*-axis) of the six objects and eliminated the objects whose positions are larger than 400 pixels from the top of the image (Figure 3e). This is based on the fact that the patient table is located at the bottom and is usually located at a position of more than 400 pixels, although a previous study has shown that a limit of 450 is sufficient to detect a patient table in many conditions.[32] The last stage of the automated

contouring was to assign all pixel within patient boundary with a value of one (Figure 3f).

The area and the mean HU of the image within the automated ROI result (i.e., patient boundary) were then calculated. The value of D_w was determined using the following equation:

$$D_w = 2\sqrt{\left[\frac{1}{1000}\overline{HU(x,y)_{ROI}} + 1\right]\frac{A_{ROI}}{\pi}} \quad (1)$$

where A_{ROI} describes the patient area in the cropped image and $\overline{HU(x,y)_{ROI}}$ is the mean HU contained in the ROI. The D_w calculation was performed for all the slices in the scanning range and an average value of D_w was calculated.

2.3 | SSDE values

The value of SSDE can be determined by normalizing the $CTDI_{vol}$ extracted from the DICOM information of the patient with the size conversion factor (f_{size}) based on Dw obtained from AAPM 204[17] and AAPM 2020.[20] SSDE value was calculated from the following equation:

FIGURE 6 Correlations between the values of D_w (a) and SSDE (b) calculated based on the old algorithm ($D_{w,o}$ and $SSDE_o$) and the new algorithm ($D_{w,n}$ and $SSDE_n$) in the chest images with both arms raised up
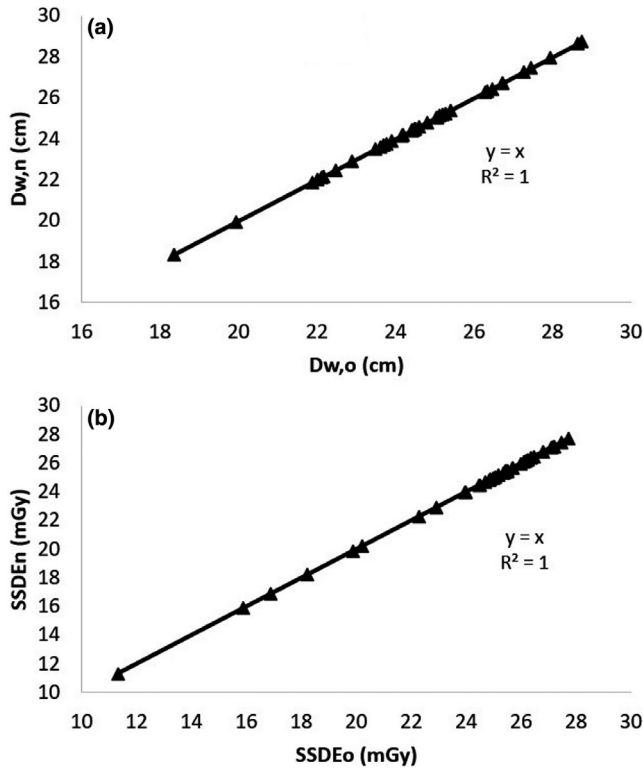

FIGURE 7 Correlations between the values of D_w (a) and SSDE (b) calculated based on the old algorithm ($D_{w,o}$ and $SSDE_o$) and the new algorithm ($D_{w,n}$ and $SSDE_n$) in the pelvic images

$$SSDE = CTDI_{vol} \times f_{size} \qquad (2)$$

The outcomes of these calculations (denoted as $D_{w,n}$ to define water-equivalent value based on the new algorithm and SSDEn to represent patient dose estimation from the new algorithm) were correlated with the results measured by the previous algorithm (old algorithm) ($D_{w,o}$ and $SSDE_o$). Both algorithms were effectively integrated into a simple graphical user interface (GUI) of IndoseCT (i.e., an in-house software for measuring SSDE) as depicted in Figure 4. The differences between $D_{w,n}$ and $D_{w,o}$ were calculated using Equation (3) and the differences between $SSDE_n$ and $SSDE_o$ were calculated using Equation (4).

$$\Delta D_w(\%) = \left(\frac{D_{w,n} - D_{w,o}}{D_{w,o}} \right) \times 100\% \qquad (3)$$

$$\Delta SSDE(\%) = \left(\frac{SSDE_n - SSDE_o}{SSDE_o} \right) \times 100\% \qquad (4)$$

3 | RESULTS

Figure 5 shows the result of our improved algorithm. All of the patient's body appearing in the image can be fully detected. The correlations of D_w and SSDE ba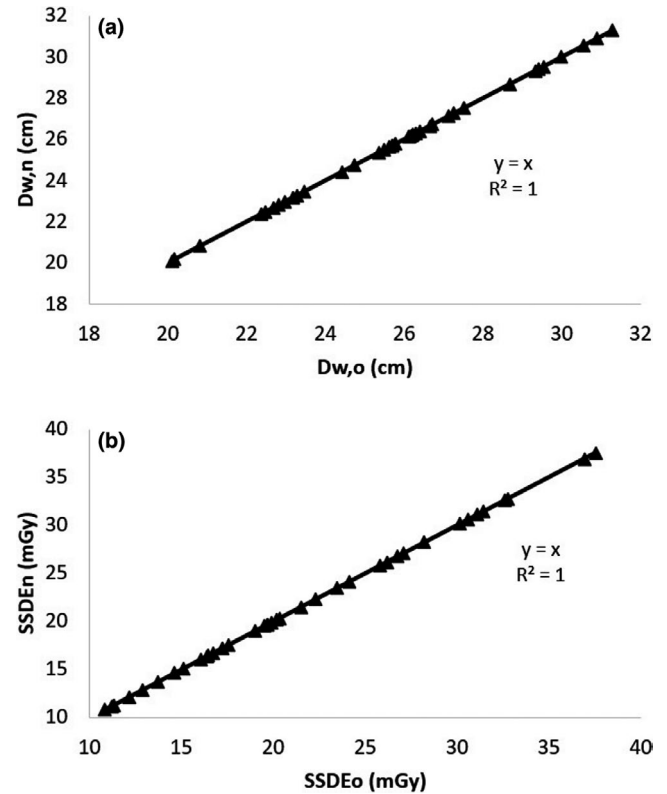sed on the previous and the new algorithms for the chest region with both arms raised up are presented in Figure 6, and for the pelvic region in Figure 7. The coefficients of linear correlation (R^2) for both regions are equal to one.

The results of D_w and SSDE based on the old and the new algorithms for images consisting of one substantial object are tabulated in Table 1. The two algorithms produce exactly the same values of D_w and SSDE, as expected.

It is interesting to analyze the results of D_w and SSDE based on the old and the new algorithms for images consisting of more than one substantial object. The correlations of D_w and SSDE values from the old and the new algorithms for the chest region with one arm down are presented in Figure 8 ($R^2 > 0.94$ for both D_w and SSDE), for the chest region with both arms down in Figure 9 ($R^2 > 0.91$ for both D_w and SSDE), and for separated leg images in Figure 10 ($R^2 > 0.99$ for both D_w and SSDE).

The differences of the results of D_w and SSDE based on the old and the new algorithms for images consisting of more than one substantial object are tabulated in Table 2. The percentage differences were averages for each dataset. The differences in the chest region with two arms down are larger than with one arm down, as predicted. Since the areas of two separated legs are comparable, the differences

TABLE 1 Results of Dw and SSDE based on the old[25] and new algorithms and their differences for various axial images consisting of one substantial object
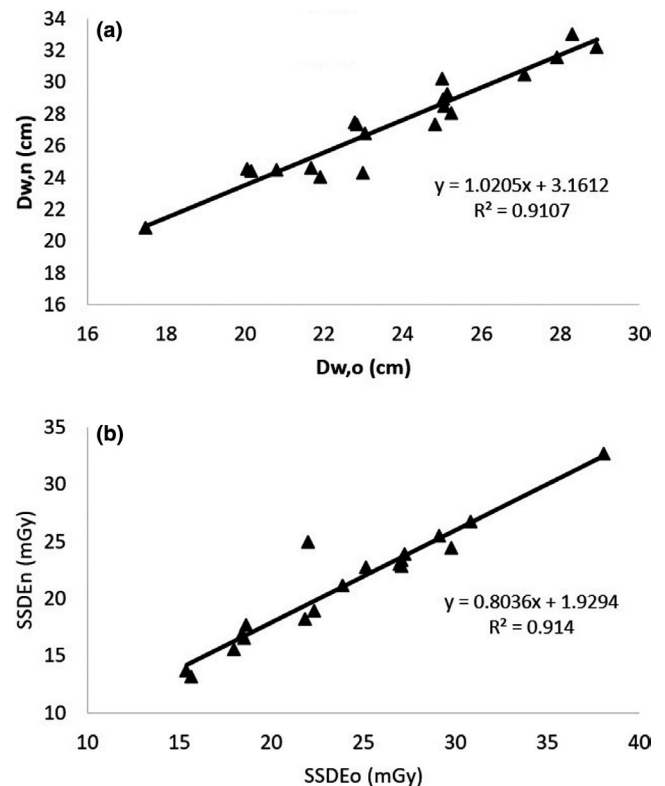
The cross-sectional image	Water-equivalent diameter (cm)		Percentage different (%)	SSDE (mGy)		Percentage different (%)
	$D_{w,o}$	$D_{w,n}$		$SSDE_o$	$SSDE_n$	
Chest + both arms raise up	24.56 ± 2.15	24.56 ± 2.15	0	24.24 ± 3.46	24.24 ± 3.46	0
Pelvic	25.77 ± 2.91	25.77 ± 2.91	0	21.81 ± 7.42	21.81 ± 7.42	0
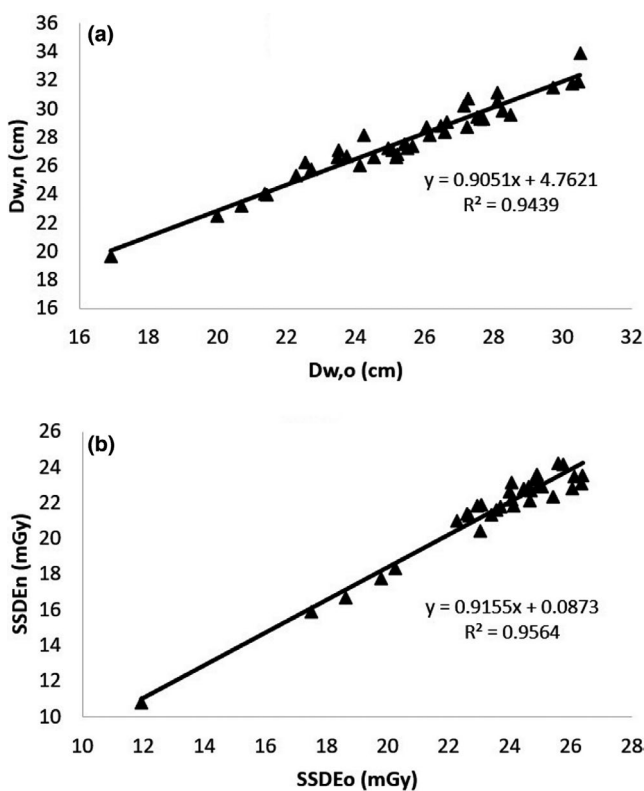
FIGURE 8 Correlation between the values of (a) D_w and (b) SSDE from the old and the new algorithm in the chest images with one arm down

FIGURE 9 Correlation between the values of (a) D_w and (b) SSDE from the old and the new algorithm in the chest images with both arms down

of D_w with the old and new algorithms is significant, that is, about 40%. It clearly shows that the calculation of D_w based on the old algorithm for images consisting of more than one substantial object gives lower D_w values than those from the new algorithm. This leads to the SSDE values calculated by the old algorithm being greater than those calculated by the new algorithm.

4 | DISCUSSION

Care should be taken in defining patient boundaries for automated calculation of D_w. The auto contouring must be able to involve all parts of the patient's body and minimize the contribution of irrelevant objects such as

the CT table. Setting the patient boundaries based on the largest object area (i.e., old algorithm[25,27]) is not sufficient for calculating D_w accurately in many clinical cases.

The inaccuracy of the old algorithm for D_w, as well as SSDE, is particularly noticeable when contouring images involving multiple body parts, which usually occurs in a clinical setting such as in an emergency condition or in radiotherapy. In an emergency CT scan, for example, traumatic patients cannot raise their arms over the heads due to trauma injuries, and have to place their arms by their side. Kweon et al.[33] showed that placing arms at the side of the body gives a higher $CTDI_{vol}$ and DLP. For this reason, we modified our previous algorithm to determine the patient contour from the six largest objects so that the

entire patient body, including separated arms or legs, can be included.

When images consist of more than one substantial object, such as chest images with arms of the patient or images with two separated legs, the new algorithm is able to detect all parts of the patient within the image. Based on the new contouring, the new algorithm gives significantly higher D_w values and lower SSDE values compared to the older algorithm. The D_w results from the new algorithm were 9.5%, 15.4%, and 39.6% higher than those from the previous algorithm for chest images with one arm placed down, both arms placed down, and images with two separated legs, respectively. The SSDE results from the new algorithm were 8.2%, 11.2%, and 20.6% lower than those from the previous algorithm for the same cases.
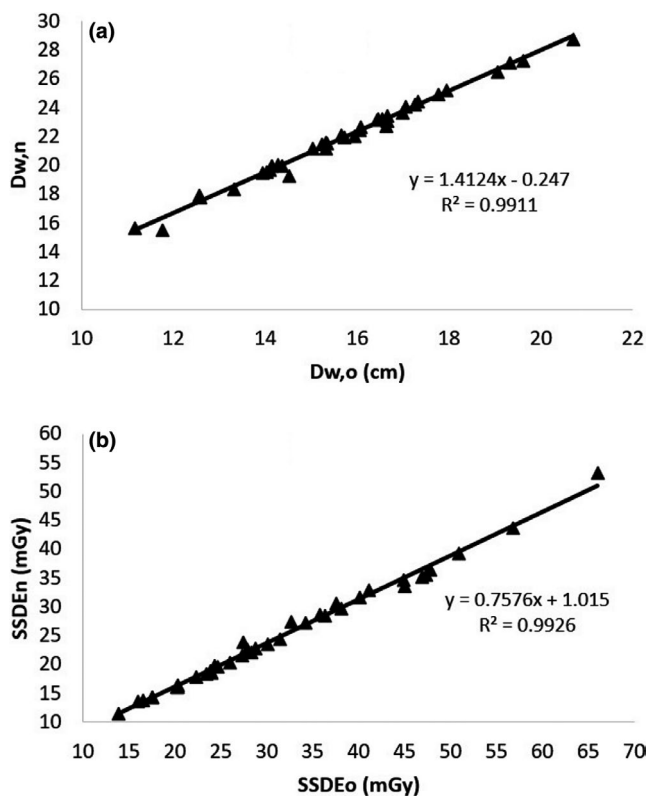

FIGURE 10 Correlation between the values of (a) D_w and (b) SSDE from the old and the new algorithm in the images containing two separated legs

The CT table may be among the six largest objects in the field of view. Previous studies have reported the impact of the CT table on the CT dose.[31,34] Li et al.[31] found that almost 12% of the total attenuation in small-sized objects comes from the presence of a CT table. Anam et al.[34] showed that the calculation of D_w with the table included in the ROI gave a higher value by 1.5%–6.2%, and the SSDE is smaller by 1.0%–5.5%, than the calculations without consideration of the patient table. In this current study, we completely excluded the attenuation contribution from the CT table, based on its position (average y-position >400 pixel). However, the position of the table can vary based on many factors, such as field of view and size of the patient. Investigation of the limit of y-position for more clinical datasets from different scanners and various field of views will be useful.

In addition, in the current study, the threshold value for segmentation is adopted from a previous study (i.e., −200 HU)[25] without any further evaluation. Although the previous study reported that this threshold value gives accurate results for the AAPM phantom, the accuracy of the threshold value for clinical images has not been established. A specific clinical image may require different threshold values to produce more accurate segmentation results. This needs a comprehensive further study. In the current study, the automated segmentation results were not compared with those of radiologist experts, so the two segmentation results were analyzed using evaluation metrics such as dice coefficients.

Detection of the six largest objects and removal of the patient table results in a more accurate measure of D_w and SSDE for all images. If the earlier algorithm was used for measuring the D_w and SSDE from images with more than one substantial object, the results can be corrected using the relationships in Figures 8–10 ($R^2 > 0.9$). The new modified algorithm is a fast and simple alternative way of providing accurate values of patient diameter and estimated dose.

5 | CONCLUSIONS

An improved automated method to calculate D_w and SSDE estimates is presented in this study. The

TABLE 2 Results of D_w and SSDE based the old[25] and new algorithms and their differences for various axial images consisting of more than one substantial object

The cross-sectional image	Water-equivalent diameter (cm)		Percentage difference (%)	SSDE (mGy)		Percentage difference (%)
	$D_{w,o}$	$D_{w,n}$		$SSDE_o$	$SSDE_n$	
Chest + 1 arm down	25.47 ± 3.00	27.81 ± 2.79	9.49 ± 3.52	23.38 ± 2.99	21.47 ± 2.78	8.19 ± 2.38
Chest + 2 arms down	23.80 ± 3.00	27.45 ± 3.21	15.35 ± 4.57	23.98 ± 5.90	21.20 ± 4.96	11.19 ± 6.81
Two legs	15.75 ± 2.12	22.00 ± 3.00	39.64 ± 2.06	31.92 ± 12.32	25.20 ± 9.37	20.55 ± 2.72

algorithm employs detection of the six largest objects within an image and deletion of the CT table. The algorithm gives the same results for D_w and SSDE as the earlier algorithm when images consist of only one substantial object. However, with images consisting of more than one substantial object, the new algorithm is able to detect all parts of a patient within the image and subsequently gives significantly higher D_w values and lower SSDE values compared to the earlier algorithm. The percentage differences of the D_w values between the new and old algorithms are 9.5%, 15.4%, and 39.6% for the chest region with one arm placed down, both arms placed down, and images with two separated legs, respectively. The new algorithm represents a more general approach for accurate D_w and SSDE estimation.

ACKNOWLEDGMENTS

CONFLICT OF INTEREST

Dr. Choirul Anam and Dr. Freddy Haryanto are IndoseCT developers. This software is not commercially available. It can be made available on request for research purposes. Rest of the authors have no conflicts of interest to disclose.

AUTHOR CONTRIBUTION

CA and FH conceived the idea. CA and FRM developed the software. WKD, HS, PT, and CA calculated the D_w and SSDE on patient images based on the developed software. WKS, CA, and GD wrote the paper. All authors approved the final version of the paper.

ORCID

Choirul Anam https://orcid.org/0000-0003-0156-6797

REFERENCES

1. Mettler FA, Bhargavan M, Faulkner K, et al. Radiologic and nuclear medicine studies in the United States and worldwide: frequency, radiation dose, and comparison with other radiation sources—1950–2007. *Radiology*. 2009;253:520-531.
2. Pearce MS. Patterns in paediatric CT use: an international and epidemiological perspective. *J Med Imaging Radiat Oncol*. 2011;55:107-109.
3. Huang W-Y, Muo C-H, Lin C-Y, et al. Paediatric head CT scan and subsequent risk of malignancy and benign brain tumour: a nation-wide population-based cohort study. *Br J Cancer*. 2014;110(9):2354-2360.
4. Masjedi H, Omidi R, Zamani H, Perota G, Zare MH. Radiation dose and risk of exposure-induced death associated with common computed tomography procedures in Yazd Province. *Eur J Radiol*. 2020;126:108932.
5. Huda W, Mettler FA. Volume CT dose index and dose-length product displayed during CT: what good are they? *Radiology*. 2011;258(1):236-242.
6. McCollough CH, Leng S, Yu L, Cody DD, Boone JM, McNitt-Gray MF. CT dose index and patient dose: they are not the same thing. *Radiology*. 2011;259(2):311-316.
7. Shope TB, Gagne RM, Johnson GC. A method for describing the doses delivered by transmission xray computed tomography. *Med Phys*. 1981;8(4):488-495.
8. Bauhs JA, Vrieze TJ, Primak AN, Bruesewitz MR, McCollough CH. CT dosimetry: comparison of measurement techniques and devices. *Radiographics*. 2008;28(1):245-253.
9. Jessen KA, Shrimpton PC, Geleijns J, Panzer W, Tosi G. Dosimetry for optimisation of patient protection in computed tomography. *Appl Radiat Isot*. 1999;50(1):165-172.
10. Boone JM. The trouble with CTDI100. *Med Phys*. 2007;34(4):1364-1371.
11. Dixon RL, Anderson JA, Bakalyar DM, et al. *Comprehensive Methodology for the Evaluation of Radiation Dose in X-ray Computed Tomography: A New Measurement Paradigm Based on a Unified Theory for Axial, Helical, Fan-beam, and Cone-beam Scanning with or without Longitudinal Translation of the Patient Table*. College Park, MD: American Association of Physicists in Medicine; 2010.
12. Dixon RL. A new look at CT dose measurement: beyond CTDI. *Med Phys*. 2003;30(6):1272-1280.
13. McCollough C, Cody D, Edyvean S, et al. *The Measurement, Reporting, and Management of Radiation Dose in CT: The Report of AAPM Task Group 23: CT Dosimetry*. College Park, MD: American Association of Physicists in Medicine; 2008.
14. Anam C, Fujibuchi T, Haryanto F, Widita R, Arif I, Dougherty G. An evaluation of computed tomography dose index measurements using a pencil ionisation chamber and small detectors. *J Radiol Prot*. 2019;39:112-124.
15. Abuhaimed A, Martin CJ. Estimation of size-specific dose estimates (SSDE) for paediatric and adults patients based on a single slice. *Phys Med*. 2020;74:30-39.
16. Strauss KJ, Somasundaram E, Sengupta D, Marin JR, Brady SL. Radiation dose for pediatric CT: comparison of pediatric versus adult imaging facilities. *Radiology*. 2019;291(1):158-167.
17. Boone JM, Strauss KJ, Cody DD, et al. *Size-specific Dose Estimates (SSDE) in Pediatric and Adult Body CT Examinations: Report of AAPM Task Group 204*. College Park, MD: American Association of Physicists in Medicine; 2011.
18. Wang J, Duan X, Christner JA, Leng S, Yu L, McCollough CH. Attenuation-based estimation of patient size for the purpose of size specific dose estimation in CT. Part I. Development and validation of methods using the CT image. *Med Phys*. 2012;39(11):6764-6771.
19. Burton CS, Szczykutowicz TP. Evaluation of AAPM reports 204 and 220: estimation of effective diameter, water-equivalent diameter, and ellipticity ratios for chest, abdomen, pelvis, and head CT scans. *J Appl Clin Med Phys*. 2018;19(1):228-238.
20. McCollough C, Bakalyar DM, Bostani M, et al. *Use of Water Equivalent Diameter for Calculating Patient Size and Size-Specific Dose Estimates (SSDE) in CT: The Report of AAPM Task Group 220*. College Park, MD: American Association of Physicists in Medicine; 2014.
21. Xu J, Wang X, Xiao H, Xu J. Size-specific dose estimates based on water-equivalent diameter and effective diameter in computed tomography coronary angiography. *Med Sci Monit*. 2019;25:71-76.
22. Anam C, Fujibuchi T, Toyoda T, et al. A simple method for calibrating pixel values of the CT localizer radiograph for calculating water-equivalent diameter and size-specific dose estimate. *Radiat Prot Dosim*. 2018;179(2):158-168.
23. Daudelin A, Medich D, Andrabi SY, Martel C. Comparison of methods to estimate water-equivalent diameter for calculation of patient dose. *J Appl Clin Med Phys*. 2018;19(5):718-723.

24. Juszczyk J, Badura P, Czajkowska J, et al. Automated size-specific dose estimates using deep learning image processing. *Med Image Anal*. 2021;68:101898.

25. Anam C, Haryanto F, Widita R, Arif I, Dougherty G. Automated calculation of water-equivalent diameter (D_W) based on AAPM task group 220. *J Appl Clin Med Phys*. 2016;17(4):320-333.

26. Özsoykal İ, Yurt A, Akgüngör K. Size-specific dose estimates in chest, abdomen, and pelvis CT examinations of pediatric patients. *Diagn Interv Radiol*. 2018;24:243-248.

27. Gharbi S, Labidi S, Mars M. Automatic brain dose estimation in computed tomography using patient dicom images. *Radiat Prot Dosim*. 2020;188(4):536-542.

28. Anam C, Haryanto F, Widita R, et al. The size-specific dose estimate (SSDE) for truncated computed tomography images. *Radiat Prot Dosim*. 2017;175(3):313-320.

29. Mihailidis D, Tsapaki V, Tomara P. A simple manual method to estimate water-equivalent diameter for calculating size-specific dose estimate in chest computed tomography. *Br J Radiol*. 2021;94:20200473.

30. Leng S, Shiung M, Duan X, Yu L, Zhang Y, McCollough CH. Size-specific dose estimates for chest, abdominal, and pelvic CT: effect of intrapatient variability in water-equivalent diameter. *Med Phys*. 2015;276(1):184-190.

31. Li B, Behrman RH, Norbash AM. Comparison of topogram-based body size indices for CT dose consideration and scan protocol optimization. *Med Phys*. 2012;39(6):3456-3465.

32. Anam C, Arif I, Haryanto F, et al. A simplified method for the water-equivalent diameter calculation to estimate patient dose in CT examinations. *Radiat Prot Dosim*. 2019;185(1):42-49.

33. Kweon DC, Choi J. Effect of arm position on image quality and radiation dose in multidetector computed tomography. *Iran J Radiol*. 2019;16(4):e86280.

34. Anam C, Haryanto F, Widita R, Arif I, Dougherty G, McLean D. The impact of patient table on size-specific dose estimate (SSDE). *Australas Phys Eng Sci Med*. 2017;40(1):153-158.